Minimal Perfusion Flow for Osteogenic Growth of Mesenchymal Stem Cells on Lattice Scaffolds

Marina Campolo
Dip. Chimica Fisica e Ambiente, University of Udine, 33100 Udine, Italy

Francesco Curcio
Dept. of Biological and Medical Sciences, University of Udine, 33100 Udine, Italy

Alfredo Soldati
Center for Fluid Mechanics and Hydraulics, University of Udine, 33100 Udine, ItalyUdine, Italy

Dept. of Energy Technology, University of Udine, 33100 Udine, Italy

DOI 10.1002/aic.14084
Published online March 26, 2013 in Wiley Online Library (wileyonlinelibrary.com)

A modeling approach to identify sets of culture conditions to promote homogeneous growth of cells in perfusion bioreactors equipped with regular shape scaffolds is proposed. We identify cases in which dynamic culturing is necessary using a zero-dimensional mass transport and reaction model. Then, based on the three-dimensional (3-D) rendering of the flow field inside the bioreactor, we identify regions where cellular growth may become critical; finally, using a 1-D mass transport and reaction model, we calculate the minimal perfusion flow necessary to maintain the cellular growth rate above a target threshold. The developed approach is used to analyze culturing conditions inside an indirect perfusion bioreactor equipped with a lattice scaffold. Regions where the perfusion flow is inadequate to foster cellular growth at the desired rate are identified. The perfusion flow required to maintain the target growth rate inside the bioreactor is calculated. © 2013 American Institute of Chemical Engineers *AIChE J*, 59: 3131–3144, 2013
Keywords: transport, diffusion, mathematical modeling, biomedical engineering, process control

Motivation and Background

The production of cellular grafts and tissues for clinical applications is currently a major challenge in regenerative medicine and tissue engineering.[1] Osteogenic cells harvested from the patient shall be expanded *in vitro* under controlled conditions to promote fast and effective production of new tissues either *in vitro* or, once reimplanted, directly *in situ*.[2] The rate at which the desired tissue can be produced *in vitro* depends on many factors: differences in cell proliferation and in cell differentiation potentials have been reported for different types of osteogenic cells [undifferentiated mesenchymal stem cells (MSC), osteoprogenitor cells, osteoblast, or osteocytes], for different isolation site and method (e.g., MSC obtained from bone marrow aspirates or from neonatal/umbilical cord blood), for donor characteristics (gender, age) and for culturing conditions (see Ref. 3 and references therein). Cell expansion is usually done in batch or continuous bioreactors equipped with scaffolds, that is, structural frameworks permeable to the culturing medium. Both the solid part (frame structure) and the permeable volume (open to the flow and available for cell growth) of the scaffold are specifically designed to support cellular growth.

Ideally, the produced tissue should be the results of a homogeneous growth which is the outcome of an initial homogeneous cell seeding and of a homogeneous cell proliferation. Consequently, the entire reactor and its operating protocols should be carefully designed to achieve a homogeneous distribution of cells during seeding, to maintain conditions which promote homogeneous proliferation and to prevent conditions which may lead to cell necrosis.

Process conditions should be tailored to the specific tissue to grow,[4,5] they might change over time and they depend on a number of variables including pH, temperature, oxygen tension, nutrient supply, and also biochemical and mechanical stimuli. As observed by Ref. 6, providing the right mechanical stimulation and adequate nutrient supply are key issues in cell culturing: at optimal operating conditions, the level of shear stress should be large enough to stimulate cell proliferation and to control their differentiation[7–9] and, yet, not too large to cause cell damage or detachment from the scaffold (see Ref. 10 among others); in addition, nutrient feeds should be large enough to replenish continuously species consumed by cellular metabolic activity.

Continuous perfusion bioreactors are advantageous compared to batch systems[11] because they offer a better control of culture conditions with minimum human manipulation. This in turn grants low contamination risk, ease of handling,

Correspondence concerning this article should be addressed to M. Campolo at marina.campolo@uniud.it

Current address of Francesco Curcio: VivaBioCell SpA, 33100 Udine, Italy

Current address of Alfredo Soldati: CISM—Centro Internazionale di Scienze Meccaniche, 33100 Udine, Italy

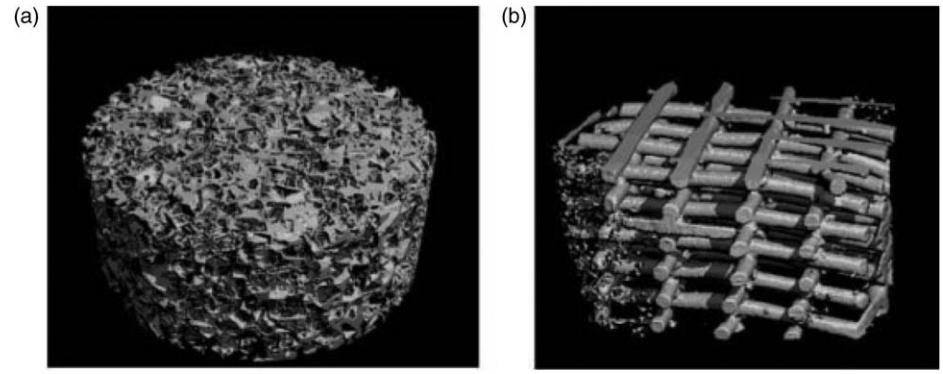

Figure 1. Types of scaffold used in tissue engineering: (a) irregular scaffold, (b) regular scaffold (from Ref. 13).

and scalability, making them the best candidates for safe, standard, and timely production of tissue constructs at the clinical scale.[12] In these systems, crucial for cell proliferation is culture microenvironment which is essentially characterized by the local values of the shear stress (i.e., mechanical stimulation) and by the local value of the species concentration. Microenvironment conditions depend strongly on the geometry of the internal frame which can be a scaffold with either irregular or regular shape.[6,13] In irregular, or random shape, scaffolds (see Figure 1a), the culture microenvironment is a complex function of the characteristics (porosity, pore-size distribution, and morphology) of the porous material constituting the scaffold and of the cell type (nutrient consumption rate). Extensive investigations have shown that the shear-stress distribution inside scaffolds with irregular perfusion channels (random size, interconnected porosity) can be calculated precisely using numerical models,[14] can be predicted *a priori* based on material properties (see Ref. 15–17), and can be controlled by adequately choosing the perfusion flow rate. Local species concentration is harder to predict because it depends both on transport rate and local consumption rate (i.e., reactivity) of species.[18] Numerical and experimental results indicate that cellular growth in irregular scaffolds can be limited by uneven distribution of nutrients which may not penetrate deep into each of the scaffold perfusion channels before being consumed by cells.[18,19]

Regular scaffolds (see Figure 1b), characterized by controlled, fully interconnected porosity, have been studied extensively in the last years as alternative to irregular porous scaffolds because they can now be easily fabricated by three-dimensional (3-D) printing, by selective laser sintering[20,21] or by microfluidic devices[22] using many different biocompatible materials. Wang et al.[22] investigated the efficacy of a 3-D, foam-like alginate scaffold with uniform pore size (250 μm) for the culture of chondrocyte for cartilage regeneration. Test results demonstrated that chondrocytes proliferated well in the alginate scaffold, maintaining their normal phenotype as healthy chondrocytes. According to Ref. 23, macropore size perfusion channels may be used to improve the medium accessibility to large part of the scaffold. 3-D numerical modeling has been used to characterize precisely culture microenvironment and can be used to derive guidelines to identify the best scaffold arrangement (size/interconnectivity of channels) for any given culture task.[24] Truscello et al.[25] used a fluid dynamics modeling approach to predict the permeability of three different regular Ti6Al4V scaffolds characterized by different pore size (500 and 1000 μm) and shape (triangular, hexagonal, rectangular) and[26] evaluated the effect of those scaffolds on the *in vitro* proliferation and differentiation of human periosteum-derived cell (hPDC); they found a significant effect of pore size (but not of pore shape) on the growth of hPDC and a concurrent effect of both pore shape and pore size on differentiation of hPDC.

Despite the high degree of complexity which can be achieved by the use of numerical simulations, simpler modeling approaches remain important for initial development and preliminary screening of new design solutions and for the identification of thresholds for the most critical culturing parameters which affect process efficiency. These models can be developed either based on data reduction approaches (e.g., the statistical analysis of *ad-hoc* designed experiments as in Ref. 27), or on basic principles.

Recently, Truscello et al.[28] developed a computationally efficient modeling approach to predict the distribution of nutrients inside a regular 2-D scaffold. The approach is based on the combined use of a 3-D numerical analysis of the unit element of the scaffold, used to obtain detailed information on the shear-stress distribution at scaffold wall, and a 1-D analytical model, used to evaluate nutrient transport along scaffold perfusion channels. In that work, the 1-D model is used to identify the influence of culture parameters on the maximum (critical) length of the scaffold construct over which an appropriate level of nutrient can be guaranteed during the culture *in vitro*. A safe, upper bound limit to perfusion flow not producing excessive shear stress on cells is identified from the results of the numerical simulation.

In this work, we propose a similar and yet more elaborated modeling approach to predict and control the distribution of nutrients in regular 3-D scaffolds. Nutrients distribution depends on feed concentration and perfusion flow, has a direct effect on cell proliferation rate and is, therefore, one of the critical parameters for bioreactor process control. Nevertheless, the efficacy of the culturing process is measured also by cell differentiation and gene-expression, which depend on cell type, chemical, biochemical, and mechanical stimulation experienced by cells during the culturing phase. Usually, mechanical stimulation is hydrodynamically induced by perfusion flow. Grayson et al.[29] examined the effect of perfusion flow velocity (i.e., shear-stress level) on the osteogenesis of human MSCs. They found that induced shear stress significantly affected cell morphology, cell–cell interactions, matrix production, and composition and the expression of osteogenic genes. Titmarsh et al.[30] observed that expansion rate, morphology, and

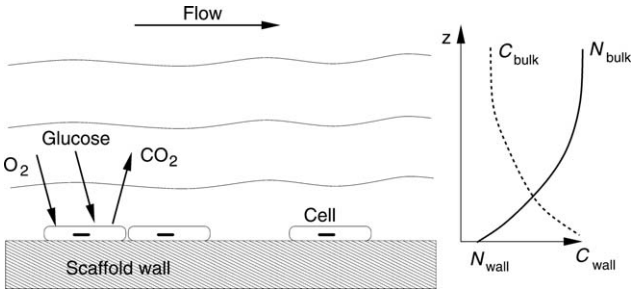

Figure 2. Cell and nutrient distribution inside a scaffold.

differentiation potential of embryonic stem cells can be optimized by tuning the medium perfusion rate. Marolt et al.[31] found that the cultivation of mesenchymal progenitors derived from human embryonic stem cells on 3-D scaffold in bioreactor using an intermediate (0.8 mm/s velocity) perfusion rate leads to the optimal formation of large and compact bone structure.

The bioreactor considered in this work is designed for the large-scale, *ex vivo* expansion of MSCs loaded on a 3-D scaffold. Scaffold shape and size can be adapted to the bone fragment to be reconstructed and, once retransplanted, cultured cells will ensure *in vivo* bone repair.[32] For the specific application under analysis, nutrients transport becomes the critical issue for process control because a minimum mechanical stimulation is required to foster cell growth and to maintain the differentiation potential. Therefore, our model is based on macroscale dimensionless transfer numbers which can be calculated based on process parameters (feed conditions, i.e., perfusion velocity and nutrients concentration, and cell metabolisms) and scaffold geometrical characteristics (construct length, perfusion channel size, and specific area). The values of these dimensionless numbers can be used to identify *a priori* conditions in which dynamic culturing becomes necessary. Then, based on a more precise characterization of the flow field and shear-stress distribution inside the bioreactor obtained by numerical analysis for the specific scaffold/bioreactor selected for culturing, a 1-D analytical model is used to identify the minimal flow rate required to guarantee the appropriate feed of nutrients to maintain the cellular growth rate above a desired, target threshold. The proposed approach is demonstrated here in an application relative to a continuous perfusion bioreactor equipped with a 3-D lattice-type scaffold. The reactor flow and shear-stress distribution is analyzed via a 3-D computational fluid dynamics (CFD) modeling, which is scaled to all flow conditions of practical interest. The reactor is currently under industrial development to grow small bone grafts from bone marrow-derived MSC (BMSC).[33]

Modeling Approach Formulation

In bioreactors used for cell culturing, process control consists of generating and maintaining suitable conditions to foster cellular growth at the desired rate driving cellular differentiation to the desired phenotype. Neglecting the direct effect of mechanical stimuli on cell and tissue growth and differentiation, at the local scale, cellular growth is a function of the number of cells and of nutrient concentrations. Even assuming that initial cell and nutrients distribution is homogeneous, the distribution of cell and nutrients may change significantly over time becoming in-homogeneous at the construct scale if perfusion flow is inadequate to feed nutrients or to remove catabolites, or to generate shear stress at cell surface higher or lower than that required for optimal mechanical stimulation.

The channel size and the degree of interconnection between perfusion channels determine the flow pattern of the medium through the construct, the shear rate and the rate at which fresh nutrients can be supplied. As demonstrated by Truscello et al.,[28] a 3-D numerical approach is necessary to quantify precisely the shear-stress distribution, whereas simpler 1-D models suffice to predict nutrients distribution through the construct. Based on these evidences, we propose a modeling approach built as follows: first, the relationship between cellular growth rate and local nutrient concentration is determined. We will use this relation to identify the threshold concentration values required to maintain the desired cell growth rate; second, a zero-dimensional model of mass transport and reaction is used to verify whether the target nutrient concentration can be met under batch (i.e., static culturing) conditions or if dynamic culturing will be required; third, based on the precise characterization of flow field and shear stress inside the specific scaffold/bioreactor derived from detailed CFD analysis, a 1-D model of mass transport and reaction of nutrients is developed and used to identify the effect of different culturing conditions on cell growth. The 1-D model is used to calculate the minimal perfusion flow rate as a function of nutrient concentration in the feed. This flow rate is required to maintain nutrient concentration above the target value at all places in the bioreactor. Each step of the approach is discussed in the following.

Cell metabolism and nutrient consumption

The proliferation and differentiation rates of cells in a culture may change significantly in space and time depending on the local number of cells and the local nutrients concentration. The local number of cells can be described by the cell surface density (i.e., number of cells per unit area). After seeding, cells are attached to the scaffold wall as sketched in Figure 2 and exposed to available flux of nutrients from the medium. The nutrient concentration in the bulk of the medium may be different from the concentration near to the scaffold wall. Differences may become very large over time in case of strong metabolic activity or insufficient perfusion. Cells will proliferate in time, consuming nutrients (mainly glucose and oxygen), and increasing their local surface density at the scaffold wall. As the cell surface density increases, cells start to compete for nutrients and for space, and a gradual reduction of the cell growth rate is observed approaching confluency. As discussed by Dunn et al.,[34] the increase of cell surface density in time over a support is described by a logistic curve

$$\frac{dC_{\text{cell}}}{dt} = KC_{\text{cell}}\left(1-\frac{C_{\text{cell}}}{C_{\text{cell,sat}}}\right) \rightarrow C_{\text{cell}} = C_{\text{sat}}\frac{1}{1+\exp\left[-Kt\right]} \quad (1)$$

where K is the growth rate (1/s), which is a function of local nutrient availability, and $C_{\text{cell,sat}}$ (cell/m^2) is cell surface density on the support at saturation (confluency). Cell density at saturation may become large enough to fill up the void of the scaffold[27] or to modify significantly the perfusion path[19] changing the scaffold permeability. Nevertheless, when the *in vitro* culturing time is reduced (e.g., 1 week)

and/or the scaffold channels are large enough (order of $1000\,\mu$m), we can safely assume that cell surface density at saturation never becomes large enough to modify significantly the thickness of the cellular layer and the permeability of the construct. In this case, an approach similar to the one adopted by Ref. 19 can be used to dynamically account for changes in the scaffold channel geometry. More complex modeling approaches based on the use of multicomponent algorithms could also be used to simulate the dynamics of the growing interface corresponding to the cellular layer.[35,36]

The functional dependence of the cellular growth rate K from (main) nutrients concentration is modeled using a Michaelis–Menten kinetic law

$$K = K_{\max} \frac{G}{K_G + G} \frac{O_2}{K_{O_2} + O_2} \tag{2}$$

where $K_{\max}$ (1/s) is the maximum cellular growth rate, K_G and K_{O_2} (mg/L or mol/L) are half-saturation constants (see Table 1) and G, O_2 (mg/L or mol/L) are the local concentrations of glucose and oxygen in the medium. Based on literature data, we assume 5.5 mM for glucose (e.g., 0.99 g/L as in $\alpha-$MEM) and up to 0.225 mM for oxygen (the oxygen saturation value at 37°C) as reference values of nutrient concentration in culturing media. However, depending on the specific culturing conditions and on scaffold geometry, cells can be exposed to nutrient concentrations orders of magnitude smaller. When local concentration of nutrients reduces, cellular growth rates also decrease accordingly, as prescribed by Eq. 2.

To complete cell expansion (i.e., to reach confluency) in a prescribed time span (larger than the minimum necessary when the growth rate is not limited by nutrient concentration), the value of cellular growth rate should be maintained above a target threshold everywhere inside the culture. The longer is the time available to complete the process, the smaller can be the growth rate target threshold. This requires in turn that the local concentration of nutrients be maintained above a critical level. To elaborate, if the aim is to complete cell expansion in 25% more time than under nutrient unlimited growth, a growth rate K larger or equal to $1/(1+25\%)K_{\max} = 80\%K_{\max}$ as culture average should be obtained inside the bioreactor; from Eq. 2, a target threshold value of concentration of each nutrient is determined as $C_t \geq 8.5 \cdot K_i$, where K_i is the nutrient half-saturation constant. Of course, growth rate may be determined by just one limiting nutrient, but this is usually oxygen due to its low solubility and diffusivity in culture media and to high cellular oxygen consumption.[28,38] Focusing on this limiting reactant, we can evaluate nutrient consumption via the flux of oxygen at scaffold wall, as

$$R(x,y,z,t) = \eta_{O_2}(t) C_{\text{cell}}(x,y,z,t) \tag{3}$$

where η_{O_2} is the oxygen consumption per cell (mol/s · cell or g/s · cell) and C_{cell} is the cell surface density (cell/m^2) which is a function of space and time. Oxygen consumption $R(x,y,z,t)$ can change in time and space depending on cell surface density and metabolic activity: values of η_{O_2} and C_{cell} can be measured experimentally. In this work, we will use the maximum value of oxygen consumption ($R_m = \max(R(t))$) to identify conservative, threshold critical conditions for oxygen distribution inside the bioreactor.

Zero-dimensional model

Perfusion channels of common regular scaffolds may vary in shape and size. From a modeling view point, we can sketch three different channel archetypes, as shown in Figure 3. Being L (m) the scaffold thickness, that is, the size of the construct in the direction not directly exposed to the fresh nutrient supply, we can have (a) close-end channels (channel length less than L), (b) open-end (i.e., perfusion) channels which extend from side to side of the construct, and (c) fully interconnected perfusion channels (i.e., channels with a lattice-like structure). Whichever of the three the shape of the channel, we can safely assume homogeneous cell seeding at scaffold wall at starting time.[6] In a zero-dimensional representation of these volumes, L is the only relevant length scale to be compared against those characteristic of transport and reaction phenomena as defined in the following.

At steady state, the local concentration of nutrients inside the control volume indicated by a dashed line in Figure 3 depends on the balance between fresh nutrients delivered by the perfusion flow and nutrients consumption at scaffold walls. The critical distance, L_{crit}, along the channel at which the concentration of the limiting nutrient will fall below the target value, C_t, can be calculated setting up the following (zero-dimensional) mass balance

$$\text{AD}\frac{C_0 - C_t}{L_{\text{crit}}} + A(C_0 - C_t)U_0 = A \cdot L_{\text{crit}} \cdot S_w R_m \tag{4}$$

where A (m^2) is the cross section of the channel, D (m^2/s) is the nutrient diffusivity in the medium, C_0 (mg/L) is the nutrient concentration at the entrance of the channel, C_t (mg/L) is the target value of nutrient concentration, U_0 (m/s) is the mean velocity of the flow inside the channel, S_w (m^2/m^3) is the specific wall area of the channel (wall surface per unit volume of fluid), and R_m (mg/m^{2}s) is the flux of nutrient

Table 1. Characteristics of Culturing Medium and Cell Metabolic Activity

Characteristics of Culturing Medium and Cell Metabolism			
Glucose concentration	G	5.5 mM	1 g/L
Oxygen concentration ($\simeq$90% sat)	O_2	0.2 mM	6.4 mg/L
Oxygen concentration at saturation (37^oC)	$O_{2,\text{sat}}$	0.225 mM	7.204 mg/L
Glucose diffusivity[a]	DG	6.600 10^{-10} m^2/s	
Oxygen diffusivity[a]	D_{O_2}	3.004 10^{-9} m^2/s	
Glucose half-saturation constant[b]	KG	0.001 ÷ 0.0012 mM	0.19 ÷ 0.22 mg/L
Oxygen half-saturation constant[b]	K_{O_2}	0.006 mM	0.192 mg/L
Glucose consumption rate[c]	η_G	378.2 ± 127.7 fmol/cell · h	
Oxygen consumption rate[c]	η_{O_2}	98.2 ± 24.2 fmol/cell · h	

[a]From Ref. 28.
[b]From Ref. 37.
[c]From Ref. 38.

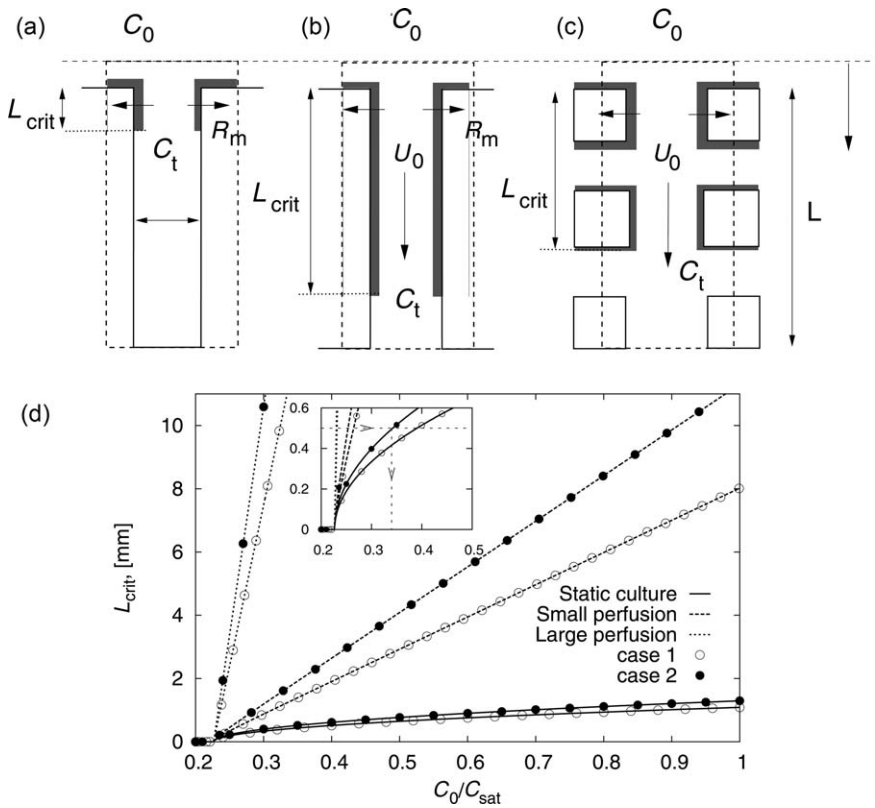

Figure 3. Alternative configurations of perfusion channels in regular scaffold: (a) close-end channel, (b) open-end (perfusion) channel, (c) lattice-like, interconnected perfusion channel; (d) functional relationship between spatial length scale, L_{crit}, dimensionless limiting nutrient concentration at channel entrance, C_0/C_{sat} for different culturing conditions: static culture (solid line), small perfusion flow rate (dashed line), and large perfusion flow rate (dotted line).

consumed at scaffold wall. In Eq. 4, the terms on the left side represent diffusion and convection while the term of the right side represents the metabolic reaction. We should remark here that the nutrient concentration at the entrance of the channel should be larger than C_t to define the critical length. The value of S_w depends on the specific geometry of the perfusion channel and can be calculated analytically for any geometrical configuration, as detailed in Appendix.

Eq. 4 can be rewritten as

$$L_{crit}^2 - \frac{(C_0 - C_t)U_0}{R_m S_w} L_{crit} - \frac{(C_0 - C_t)D}{R_m S_w} = 0 \tag{5}$$

which is a quadratic equation in L_{crit}. The only possible (physically significant) solution is given by

$$\begin{aligned} L_{crit} &= \frac{(C_0 - C_t)U_0}{2R_m S_w} + \sqrt{\left(\frac{(C_0 - C_t)U_0}{2R_m S_w}\right)^2 + \frac{(C_0 - C_t)D}{R_m S_w}} \\ &= \frac{(C_0 - C_t)U_0}{R_m S_w}\left(\frac{1}{2} + \sqrt{\left(\frac{1}{2}\right)^2 + \frac{R_m S_w D}{(C_0 - C_t)U_0^2}}\right) \end{aligned} \tag{6}$$

The critical length depends on the balance among advection, diffusion, and reaction. For a close-end channel, where $U_0 = 0$ and transport is controlled by diffusion, we get

$$L_{crit} = L_{diff} = \sqrt{\frac{(C_0 - C_t)D}{R_m S_w}} \tag{7}$$

whereas for an open-end channel, where $U_0 > 0$ and transport is controlled by advection, we get

$$L_{crit} = L_{adv} = \frac{(C_0 - C_t)U_0}{R_m S_w} \tag{8}$$

Values of L_{diff} and L_{adv} calculated for two alternative geometrical configurations of scaffold channels are summarized in Table 2. The two configurations differ for the values of specific wall area and void fraction (see Appendix for details): the first configuration (Case 1) is a scaffold with square, parallel perfusion channels; the second configuration (Case 2) is a scaffold with square, lattice-type, interconnected perfusion channels.

For the reference operating conditions listed in Table 2, the diffusion length scale is order 1 mm. The advection length scale is two orders of magnitude larger when the large perfusion rate is considered. In general, L_{crit} is a function of culture parameters (nutrient concentration at channel inlet, C_0, and perfusion flow rate or velocity, U_0), which should be tuned to meet any specific culture target. The variability of L_{crit} as a function of nutrient concentration at channel inlet (x axis) is shown in Figure 3d for a static culture (solid line, null perfusion flow rate), and for two dynamic cultures, corresponding to a small perfusion flow rate (dashed line) and a large perfusion flow rate (dotted line), respectively. Open and closed symbols identify the two different types of open-end channels. Because the effect of metabolic reaction is represented by the product $R_m \cdot S_w$, curves with symbols

Table 2. Reference Operating Conditions for Perfusion Bioreactor

Reference Operating Conditions for Perfusion Channel			
Channel size	d	1.25 mm	
Fiber/wall size	d_f	1.00 mm	
Scaffold length	L	10.00 mm	
Advective velocity[a]	U_0	2. 10^{-4} m/s	
Nutrient concentration (O_2[b])	C_0	85%C_{sat}; 6.12 10^{-3} kg/m^3	
Nutrient target concentration (O_2[b])	C_t	8.5K_{O_2}; 1.632 10^{-3} kg/m^3	
Nutrient diffusivity (O_2[b])	D	3.10^{-9}m^2/s	
Nutrient specific flux wall (O_2[b])	R_m	4.42 10^{-9} kg/m^2s	
Scaffold type		**Case 1 // Channels**	**Case 2 Lattice**
Specific wall surface	S_w	3200 m^2/m^3	2258 m^2/m^3
Void fraction	ε	30.86%	58.29%
Diffusion length scale	L_{diff}	0.976 10^{-3} m	1.162 10^{-3} m
Advection length scale	L_{adv}	0.0635 m (LP)	0.0899 m (LP)
Peclet number (macro)	Pe_L	666.67 (LP); 66.67 (SP)	
Damkholer number (macro)	Da_L	104.97	74.10
Peclet number (micro)	Pe	83.33 (LP); 8.33 (SP)	
Damkholer number (micro)	Da	1.64	1.158

[a]Velocity value for large Perfusion (LP). Velocity for small Perfusion (SP) is $0.1 \cdot U_0$.
[b]Limiting reactant.

may also represent the effect of a change in the nutrient reactivity R_m for one type of channel (Case 1, small R_m; Case 2, larger R_m). The close up of the graph shown in the inset shows that $L_{diff} \propto (C_0 - C_t)^{0.5}$ for diffusion-controlled transport, whereas $L_{adv} \propto (C_0 - C_t)U_0$ for advection controlled transport. According to data in Table 2, when $C_0 = 0.85 \cdot C_{sat}$ the diffusion length is $L_{diff} = 0.976$ mm for Case 1 ($L_{diff} = 1.162$ mm for Case 2) indicating that a static culturing protocol is inadequate to culture cell over any construct of thickness $L > L_{diff}$. As shown by the solid line in Figure 3b, depending on the value of C_0/C_{sat}, static culturing can be effective for scaffolds up to order 1mm thick. To elaborate, if $L_{crit} = 0.5$ mm, $C(0)/C_{sat}$ should be at least 39% to ensure nutrient supply ($C > C_t$) in Case 1 (34% in Case 2); cell culturing on thicker supports becomes possible only if dynamic perfusion is used: for a given construct thickness, concentration at channel inlet can be smaller than that required by a static culture.

To identify conditions in which dynamic culturing becomes necessary and to ensure adequate nutrient delivery, we can rewrite Eq. 6 in dimensionless form. Using the advection length scale for reference and introducing two-dimensionless parameters, the Damkholer number $Da_L = R_m S_w L_{crit}^2 / D(C_0 - C_t)$, and the Peclet number $Pe_L = U_0 L_{crit}/D$, we obtain

$$\frac{L_{crit}}{L_{adv}} = \frac{Da_L}{Pe_L} = \frac{1}{2}\left(1 + \sqrt{1 + 4\frac{Da_L}{Pe_L^2}}\right) \tag{9}$$

The subscript L identifies the macroscopic length scale (corresponding to the scaffold/construct thickness) at which dimensionless parameters are calculated. In Figure 4, we show the dimensionless parameters space described by macroscale Peclet and Damkholer numbers; the thick line represents pairs of (Pe_L, Da_L) values which satisfy Eq. 9, that is, transport/reaction conditions for which a critical length exists. The equation of the line is $Da_L = Pe_L + 1$; the plot is shown using a log-log scale. Values of (Pe_L, Da_L) which lie above the line identify reaction-controlled situations; values which lie below the line identify transport-controlled situations. As shown in Figure 4b, L_{crit} tends obviously toward the advection scale when the problem is advection controlled ($Pe_L > 1$). When advection is very small ($Pe_L < 1$), L_{crit} may be orders of magnitude larger than the (very small) advection scale thanks to diffusion, but this transport mechanism is effective only at small scales.

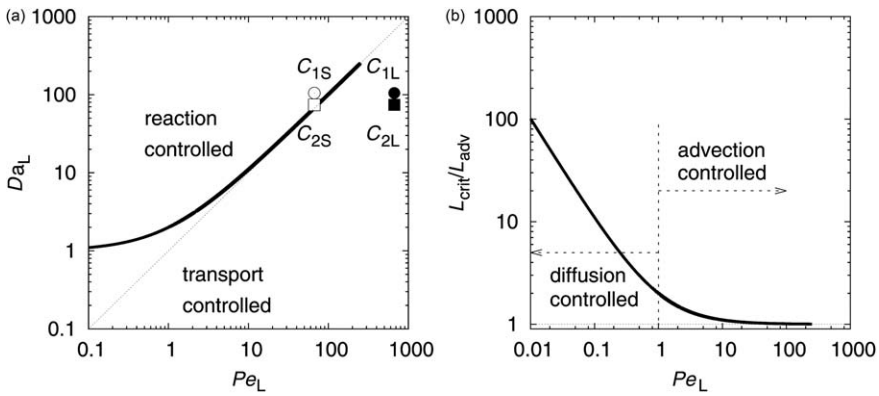

Figure 4. Critical length for transport/reaction-controlled situations: (a) couples of (Pe_L, Da_L) for which a finite critical length exists (thick black line); (b) value of the critical length at different flow regimes.

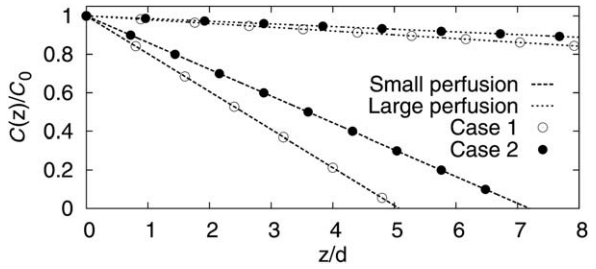

Figure 5. Concentration profile along perfusion channel: small perfusion (dashed line) and large perfusion (dotted line); parallel perfusion channel (Case 1, empty circle) and interconnected perfusion channel (Case 2, solid circle).

With reference to the cell culturing application, the objective is to fix the operating parameters of a perfusion bioreactor (flow velocity, U_0, and feed concentration, C_0) so that reaction is not the controlling phenomenon at the scale of the scaffold/construct thickness, L. When $L > L_{\text{diff}}$, the static culture protocol ($U_0 = 0$, $Pe_L = 0$) is ineffective because culture microenvironment is controlled by reaction. To ensure adequate cell colonization, advection shall support diffusion and perfusion bioreactors shall be used. Choosing operating conditions represented by pairs of (Pe_L, Da_L) which lie below the line in Figure 4 ensure that reaction will be not the controlling phenomenon at the scale of the scaffold/construct thickness. Consider for instance operating conditions listed in Table 2 corresponding to small perfusion flow through parallel perfusion channels (point C_{1S} in Figure 4). Point C_{1S} lies above the line, indicating that reaction is controlling and $L_{\text{crit}} < L$. To move from a reaction controlled into a transport-controlled situation, we can either increase perfusion flow and velocity, U_0, increasing the value of Pe_L and moving to the right to point C_{1L}, or we can change scaffold geometry or type of cell culture, decreasing the product $R_{\text{m}} \cdot S_{\text{w}}$, reducing Da_L and moving down from C_{1S} to C_{2S}. Large perfusion rates and advection velocities shall be used to transport nutrients deeper into channels, or to compensate for small nutrients concentration in the feed and to replenish efficiently nutrient concentration in case of intense metabolic activity (large species reactivity).

1-D model

The zero-dimensional model developed in the previous section can help to identify the threshold between static or dynamic feed protocols but is of course ineffective in determining local growth situations which may become problematic under either of the two feeding protocols. Again referring to the schematics of Figure 3, if we identify with z the coordinate along the perfusion channel, the mass balance equation at steady-state condition can be rewritten using a 1-D model approach as

$$0 = -U_0 A \frac{dC}{dz} + AD \frac{d^2C}{dz^2} - S_{\text{w}} A R_{\text{m}}, \tag{10}$$

where all variables are defined as before. Using C_0 as the reference concentration and $d = \sqrt{A}$ as the reference length scale, Eq. 10 in dimensionless form becomes

$$\frac{d^2\tilde{C}}{d\tilde{z}^2} - Pe \frac{d\tilde{C}}{d\tilde{z}} = Da, \tag{11}$$

where the tilde identifies dimensionless variables, $\tilde{z}$ is the spatial coordinate, $\tilde{C}$ is the limiting nutrient concentration, $Pe = U_0 d/D$ is the Peclet number, and $Da = R_{\text{m}} S_{\text{w}} d^2/(C_0 - C_t)D$ is the Damkohler number. In Eq. 11, Pe and Da are defined using the size of the channel as reference length scale (microscale). Boundary conditions for Eq. 11 are $\tilde{C}(0) = 1$ ($C(0) = C_0$) and $d\tilde{C}/d\tilde{z}(\tilde{L}) = 0$ where $\tilde{L}$ is the (dimensionless) length of the perfusion channel. The equation can be solved to calculate the concentration profile along the channel, $\tilde{C}(\tilde{z})$. If $Pe > 0$

$$\tilde{C}(\tilde{z}) = \left[1 - \frac{Da}{Pe^2}\exp\left(-Pe\tilde{L}\right)\right] - \frac{Da}{Pe}\tilde{z} + \frac{Da}{Pe^2}\exp\left[-Pe\left(\tilde{L} - x\right)\right] \tag{12}$$

The concentration profiles along the channel for different values of Pe (i.e., small/large perfusion) and Da (i.e., small/large channel specific area or nutrient reactivity) are shown in Figure 5. Parameters used for the calculation are those listed in Table 2. Concentration profiles are monotonically decreasing along the channel, with the larger decreasing rate for smaller Pe (i.e., small perfusion). For a fixed value of Pe, the concentration is everywhere smaller when Da increases. The rate of change of concentration is almost linear, at least for the range of values considered for Da and Pe. Rather expectedly, the lowest concentration is always found at the end of the channel where

$$\begin{aligned}\frac{C(L)}{C_0} &= \tilde{C}\left(\tilde{L}\right) = 1 - \frac{Da}{Pe}\tilde{L} - \frac{Da}{Pe^2}\exp\left(-Pe\tilde{L}\right) \\ &= 1 - \frac{Da}{Pe}\tilde{L}\left[1 + \frac{1}{Pe_L}\exp\left(-Pe_L\right)\right] = 1 - \frac{Da}{Pe}\tilde{L}\left[1 + f(Pe_L)\right]\end{aligned} \tag{13}$$

with $Pe_L = Pe \cdot \tilde{L}$ defined as the product between the microscale Peclet number and the dimensionless channel length. As already predicted by the zero-dimensional model, at small perfusion flow, we can not ensure sufficient nutrient feed up to the end of the perfusion channel. However, the 1-D model can be used to calculate how process conditions should be changed to meet the target. Equation 13 is a relationship between $\tilde{C}\left(\tilde{L}\right)$, Da, and Pe. Da is a function of the entrance surplus concentration, $C_0 - C_t$, and nutrient reactivity, R_{m}, while Pe is a function of velocity, U_0, and flow rate, Q. Equation 13 has been derived assuming steady state, constant velocity, and constant reactivity along the channel and can be applied to perfusion channels of any shape (parallel channels, interconnected channels and also channels with irregular shape) provided that U_0 and S_{w} can be conservatively estimated and/or do not change significantly along the perfusion path.

The contribution of $f(Pe_L)$ becomes rapidly negligible as Pe_L increases: $f(Pe_L) \simeq 1$ for $Pe_L = 0.5$ and $f(Pe_L) \simeq 0$ for $Pe_L \geq 3$. Therefore, for $Pe_L \geq 3$ Eq. 13 can be simplified as

$$\frac{C(L)}{C_0} \simeq 1 - \frac{Da}{Pe}\tilde{L} \tag{14}$$

The variation of the dimensionless concentration at the outlet of a channel (given length $\tilde{L} = 8$) is shown in Figure 6a as a function of Pe and Da numbers. Predictions obtained using Eq. 13 (full model) or 14 (first order model) are

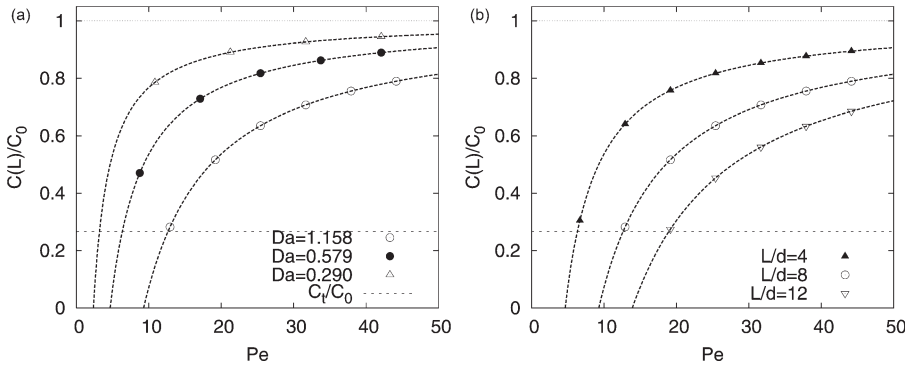

Figure 6. Variation of dimensionless concentration of limiting nutrient at outlet of channel for different perfusion condition, *Pe*: (a) fixed length $\tilde{L} = 8$, different values of *Da*; (b) fixed $Da = 1.158$, different length of scaffold channel; dashed line represents target concentration to guarantee (at least) $K = 80\%K_{max}$ all along the channel.

perfectly superimposed. Consider first the profile obtained for $Da = 1.158$ (empty circles). The model shows that, to have $\tilde{C}_t = C_t/C_0 \geq 0.266$ (and $K \geq 80\%K_{\max}$) at all locations including the end of the channel, the *Pe* number should be at least 12.63. If *Da* is halved (i.e., species reactivity is reduced), *Pe* can be as small as 6.31; if *Da* is halved again, *Pe* can be as small as 3.16, all in a linear proportional fashion (Eq. 14).

The variation of the dimensionless concentration at the outlet of a channel when *Da* is fixed ($Da = 1.158$) and the channel length changes ($\tilde{L} = 4$, 8 and 12) is shown in Figure 6b. If the channel length decreases (solid triangles) *Pe* can be reduced to 6.31; if the channel length increases (open triangles), *Pe* should be increased to 18.94. The relationship between culturing parameters to ensure a target growth rate (*Pe* and $C(L)/C(0)$) for any cell type and scaffold geometry (*Da* and $\tilde{L}$) can be written in explicit form as

$$Pe_{\min} = \frac{Da \cdot \tilde{L}}{1-\tilde{C}_t} \tag{15}$$

This equation may be used as a process control equation to fix the flow rate necessary to keep the nutrient concentration at outlet of each channel above a given limit $\tilde{C}_t$.

Case Study

The model proposed in this work was used in the early stage of development of one scaffold/bioreactor specifically designed to grow small bone grafts (see patent WO 2011/073261 A2). The objective was to identify any potential deficiency in bioreactor/scaffold design and in the culturing protocol. As described previously, first we calculated the macroscale dimensionless transfer numbers. Then, we used the computational analysis to characterize culture microenvironment, that is, the shear-stress distribution at scaffold wall, responsible for mechanical stimulation of cells, and local flow conditions through the scaffold perfusion channels, which control the nutrient supply. Finally, we calculated the minimal perfusion flow necessary to keep the nutrient concentration above the target limit to ensure cellular growth at the desired rate. Preliminary *in vitro* and *in vivo* (mice and rabbit) toxicity and efficacy tests have been completed successfully for bone grafts produced using the scaffold/bioreactor and the culturing protocol analyzed in this work; animal preclinical trial (sheep) are currently in progress.

Configuration of scaffold/bioreactor

The bioreactor and scaffold investigated are shown in Figure 7. Geometrical dimensions are summarized in Table 3. The scaffold is a lattice-like structure (see Figure 7b) made of a mixture of polycaprolactone and tricalcium phosphate fixed inside the main bioreactor chamber by a central, cylindrical hollow pipe which fits onto a cylindrical support. The scaffold is made of square fibers arranged in a $5 \times 5 \times 5$ matrix. The fiber inter distance is 1.25 times the fiber dimension (1 mm). A gap is available around the scaffold (1 mm thick) for fluid flow.

Culture conditions are summarized in Table 4. According to the culturing protocol, BMSC are homogeneously seeded on scaffold walls at starting time (dynamic seeding by pipetting onto scaffold surface and slow rotation of scaffold/bioreactor assembly at zero-perfusion flow); the homogeneity of cell distribution on scaffold walls after seeding was evaluated during preliminary tests using stereomicroscopy and live/dead staining; then, a water solution of glucose, oxygen, and growing factors (low human serum percent (HS%) medium[39]) is fed continuously to the culture (1ml/min perfusion flow rate). Glucose concentration in the feed is $G = 1$ mg/ml (5.5 mM), high enough to avoid any nutrient limiting effect to the cell culture, but not too high to produce toxic effect on cellular growth.[40] Dissolved oxygen concentration in the inlet stream is maintained at least equal to 80% of the saturation value ($O_2 \geq 5.76$ mg/L, 0.180 mM). Biochemical and biophysical analyses of cultured cells were made at the end of the culturing process as described in Ref. 41.

Evaluation of cell metabolism and nutrient consumption

Experimental tests were performed in a batch bioreactor maintained at $T = 37 \pm 0.1$°C to evaluate cell metabolic activity, that is, cell growth rate and nutrients consumption over time. Cells were seeded inside a medium (glucose concentration 1 mg/mL, that is, 5.5 mM, oxygen concentration 85−95% of the saturation value) and, after each day, their growth was evaluated sampling the medium from wells of known area (3.4 cm^2). Some wells were harvested to generate cell numbers. Every day the medium was changed using a fresh supply of the same medium, and the residual glucose

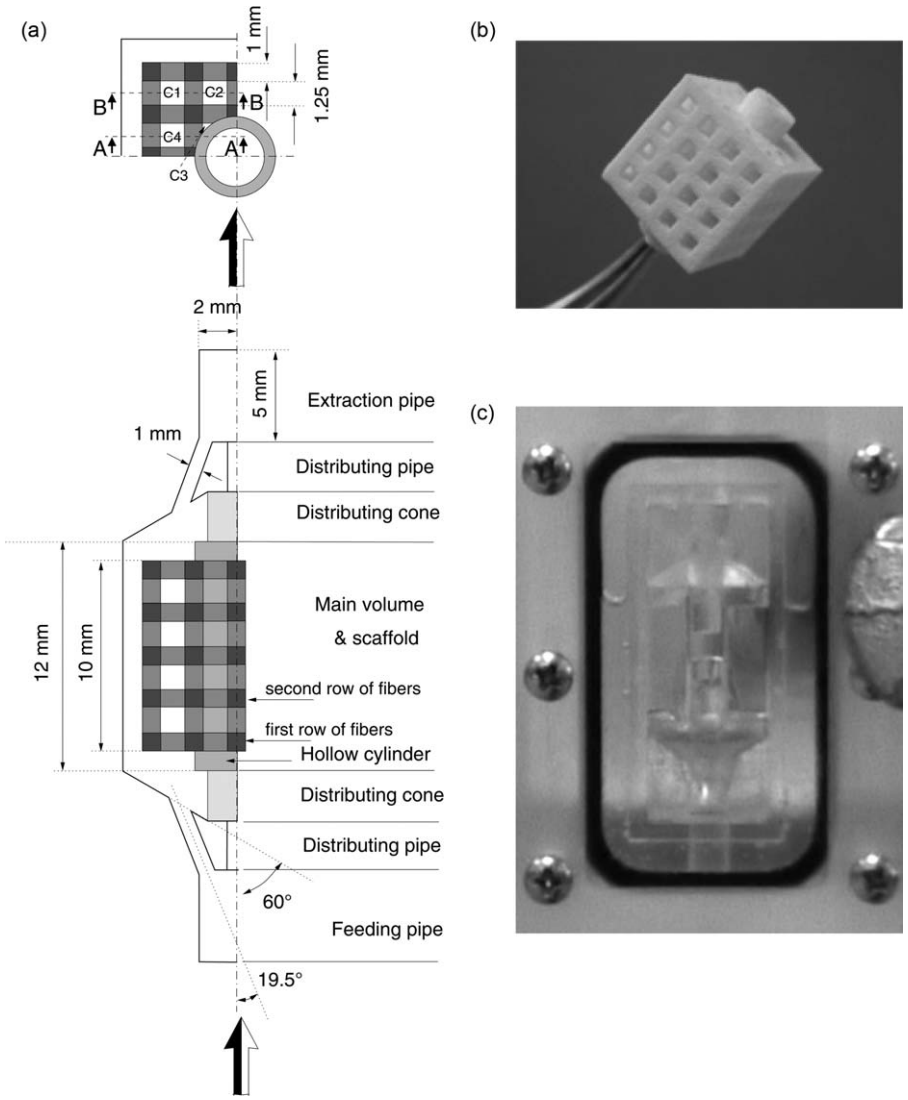

Figure 7. Bioreactor geometry: (a) sketch of bioreactor/scaffold configuration (domain simulated by computational analysis), (b) lattice-type scaffold, and (c) empty bioreactor.

was measured to evaluate glucose consumption. Experimental data showed saturation of cell density after 1 week.

From the analysis of experimental data, we estimated the maximum glucose consumption equal to $\eta_G = 416$ fmol/cell·h and cell surface density at saturation $C_{\text{cell,sat}} = 10^{10}$ cell/m^2. Data from our experiment are in good agreement with measurements made for MSC by Ref. 37, who report values of glucose consumption in the range $\eta_G = 378.2 \pm 127.7$ fmol/cell · h for $C_{\text{cell}} < 10^5$cells/cm^2. According to Ref. 37, oxygen consumption is not stoichiometric, with $\eta_{O_2} = 98.2 \pm 24.2$ fmol/cell · h. Combining the value of η_{O_2} from Pattappa et al. (2011) with cell surface density data from

Table 3. Geometrical Dimensions of Bioreactor under Study

Geometrical Dimensions of Bioreactor		
Inlet/outlet pipe diameter	D_{feed}	4 mm
Distributing pipe diameter	D_{distr}	1 mm
Number of distributing pipes	N_{distr}	4
Inclination of distributing pipes	β	19.5°
Cone angle	α	60°
Bioreactor half width	W	6 mm
Bioreactor length	L	12 mm
Scaffold dimension	$L_x \times L_y \times L_z$	$10 \times 10 \times 10$ mm
Fiber size	d_{f}	1 mm
Fiber interspace	d	1.25 mm
Fiber number	N_{f}	$5 \times 5 \times 5$
Inner cylinder	d_{in}	3 mm
Scaffold cylinder	d_{sc}	4 mm

Table 4. Nominal Operating Conditions of Bioreactor under Study

Nominal Operating Conditions		
Flow rate	Q_n	1 cm^3/min
Temperature	T	37°C
Glucose conc.	G	1 mg/mL, (5.5 mM)
Oxygen conc.	O_2	5.763 mg/L (0.180 mM, 80%C_{sat})
MSC		
Cell density seeding	C_{cell}	8.10^8 cell/m^2
Cell density saturation	$C_{\text{cell,sat}}$	1.10^10 cell/m^2
Maximum glucose consumption	η_G	416 fmol/cell h
Peak O_2 consumption[a]	$R_{O_2,m}$	4.42 10^{-9} kg/m^2s
Max growth rate	$K_{\max}$	0.88 day^{-1}

[a]Calculated from Eq. 3 using η_{O_2} from Ref. 37 and $C_{\text{cell,sat}}$ measured during experiments.

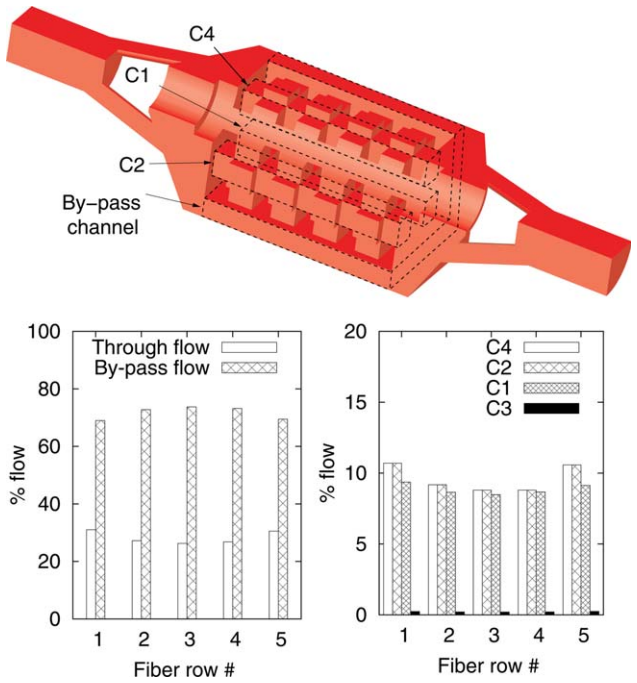

Figure 8. 3-D computational domain (a), and flow partitioning inside the bioreactor: (b) fraction of flow around/across the scaffold; (c) fraction of flow along scaffold channels.

[Color figure can be viewed in the online issue, which is available at wileyonlinelibrary.com.]

our experiment, we estimated a peak oxygen consumption equal to $R_{\mathrm{m}} = R_{O_2} = 4.42 \cdot 10^{-9} \mathrm{kg/m^2 s}$.

3-D flow field analysis

The flow field inside the bioreactor was investigated numerically using a commercial finite volume solver of the fluid transport equations (StarCD®). At nominal operating conditions, the flow is in the creeping regime at all locations in the bioreactor, with Reynolds number (based on local mean velocity and length scale) everywhere less than 1. In this regime, viscous forces prevail over inertial forces, and all flow processes are controlled by the linear terms of the Navier–Stokes equations. Via proper linear scaling, one single-flow simulation is, therefore, sufficient to represent all flow conditions of practical interest: any change of the perfusion flow will produce a linear change of local velocity and shear stress.

We performed one single-numerical simulation at the nominal perfusion flow rate ($Q_n = 1$ cm^3/min) considering one fourth of the bioreactor, the minimal periodic part of the domain. The computational domain is shown in Figure 8a. In the present geometrical configuration, the flow may follow two specific preferential paths inside the bioreactor, moving either through the scaffold (along the main scaffold channels C1, C2, C3, and C4 also shown in Figure 7a, aligned with the reactor axis, z, and characterized by an hydraulic diameter $D_H = 1.25$ mm) or through the gap around the scaffold ($D_H = 2$ mm). The Poiseuille law ($\Delta p \propto Q/D_H^4$) predicts that a larger fluid proportion (69%) flows around the scaffold. In Figure 8b, we show the percent values of flow moving along the main scaffold channels (through flow) and through the gap around the scaffold (by-pass flow calculated from the numerical simulation). Values are calculated at different z locations, taken each one across one row of fibers. In Figure 8c, we show the percent value of flow moving along each main scaffold channels. Results show that about 70% of the fluid flows through the gap around the scaffold; this figure increases slightly ($\simeq 5\%$) moving to the center of the bioreactor. The flow through the main scaffold channels exhibits an opposite trend, decreasing to a minimum value at the center of the scaffold. The flow through the different scaffold channels is not the same; as shown in Figure 8c, channel C3, the nearest to the central cylinder and with the smaller cross section (see Figure 7a), delivers only 0.2% of the overall perfusion flow; channels C2 and C4, which are symmetric, deliver each up to 11% of the overall perfusion flow; channel C1, near to the outer corner, delivers about 9.5% of the overall perfusion flow. The flow delivered along each channel decreases moving to the center of the bioreactor (up to 8.48% in channel C1) and increases again after this point; the percent flow reduction (less than 10% relative to flow at channel inlet) indicates fluid (and mass) exchange through the side vanes connecting the main scaffold channels.

A simplified, conservative representation of the complex, 3-D perfusion path which controls nutrient supply in the different regions of the scaffold can be obtained considering the perfusion flow splitted among the gap around the scaffold and the four, parallel, weakly interconnected main channels, each one delivering a different flow rate. The flow rate may be conservatively assumed equal to $8.48\% Q_n$ (i.e., minimum value inside the scaffold) for channels C1, C2, and C4 and equal to $0.2 Q_n$ for Channel C3; side vanes along each channel will be conservatively modeled as dead zone regions in which the transport of oxygen and glucose will be ultimately controlled by diffusion. This modeling scheme will be used to evaluate the effect of nutrient transport inside the bioreactor.

3-D shear-stress distribution

The shear stress experienced by cells is a crucial parameter to control cell growth and differentiation. It is beyond the purpose of this work to model explicitly the effect of shear-stress level on the local cellular growth rate and differentiation. In this work, numerical simulations are used to verify whether the shear stress at cell surface is locally higher or lower than that required for optimal mechanical stimulation. In Figure 9a, we show isocontours of shear stress calculated in the entrance region of main channel C2. Only a short length of the channel is shown, corresponding to the first row of fibers and side vanes. In this region, the perfusion flow rate is the largest and the largest shear rate is also expected. Values of shear stress are shown in dimensionless units; the reference value of shear stress, $S_{\mathrm{ref}} = 4.432 \cdot 10^{-10} \mathrm{N/mm^2}$, is calculated as follows

$$S_{\mathrm{ref}} = \mu \frac{U_{\mathrm{ave}}}{d/2} \tag{16}$$

where U_{ave} is the (uniform) section averaged velocity in the main chamber of the bioreactor ($U_{\mathrm{ave}} = Q_{\mathrm{n}}/A_{\mathrm{mc}}$), $A_{mc} = 60$ mm^2 is the through flow area of the main chamber of bioreactor, d is the channel size, and μ is fluid viscosity. As expected, the largest values of shear stress are found at the inlet and outlet border of each fiber (red color); the

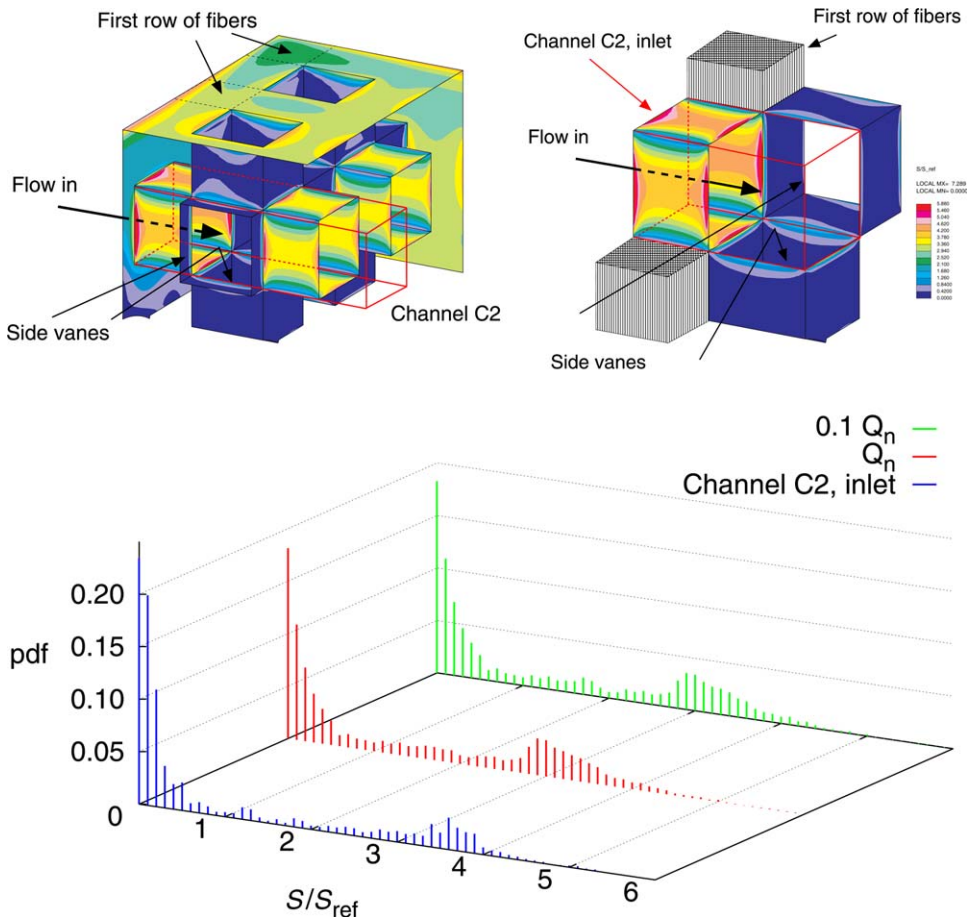

Figure 9. Shear-stress distribution at scaffold wall: (a) dimensionless shear-stress isocontours at the scaffold inlet (left) and detail of shear-stress distribution at inlet of Channel C2 (right); (b) probability density function of dimensionless shear stress at the entrance of Channel C2 (blue histogram), over the entire scaffold surface at nominal perfusion flow rate (red histogram) and at reduced ($0.1 \cdot Q_n$) perfusion flow rate (green histogram).

[Color figure can be viewed in the online issue, which is available at wileyonlinelibrary.com.]

minimum values (pale and dark blue colors) are found in the corners of the channel and at the surface of side vanes.

The probability density function (PDF) of shear-stress distribution at scaffold surface is shown in Figure 9b. Three different PDF curves are shown, corresponding (from bottom to top) to the shear-stress distribution in the portion of channel shown in Figure 9a (in blue), the shear-stress distribution calculated over the entire scaffold surface at nominal perfusion flow (in red), and the shear-stress distribution calculated over the entire scaffold surface when the perfusion flow is reduced to $0.1 \cdot Q_n$ (in green). Consider first the blue histogram: the PDF indicates that small values of shear stress are the most frequent at scaffold wall (blue isocontours in Figure 9a). The second peak in the PDF identifies the second most frequent range of values, corresponding to orange regions in Figure 9a. The shape of the red histogram is very similar to the blue one. The second peak of the PDF is shifted toward lower values of shear stress because in the regions of the scaffold represented in Figure 9a, the perfusion flow is locally larger. The green histogram, calculated when the perfusion flow rate is reduced to $0.1Q_n$, superposes almost perfectly to the red one: we are in the creeping regime and the shear-stress distribution scales linearly with the perfusion flow.

For the nominal flow rate, the calculated shear stress is in the range $0.43 \cdot 10^{-12} \div 0.32 \cdot 10^{-8}$ N/mm^2, which is within the values ($8 \div 30$ dyne/cm$^2 = 8 \cdot 10^{-7} \div 30 \cdot 10^{-7}$N/mm^2) reported in the literature for the excitation of osteocytes.[6] These values are well-below the values ($10^{-6} \div 10^{-4}$N/mm^2) reported to detach cells in 2-D[10] and in the lower range of the values ($10^{-9} \div 10^{-7}$N/mm^2) which are reported to be responsible for detachment in highly porous, 3-D scaffold (mean pore size of 325, 120, and 85 μm).[10] Values are at least one order of magnitude less than those (0.92 dynes/cm$^2 = 0.92 \cdot 10^{-7}$N/mm^2) reported to be detrimental for cellular growth.[8] This indicates that mechanical stimulation is not to be considered a limiting factor for cellular growth in the present configuration.

Minimal perfusion flow

Local availability of oxygen is the only significant factor controlling cellular growth in the bioreactor under study. Therefore, we focused on the simplified, 1-D representation of the perfusion path derived from the numerical analysis to identify the minimal perfusion flow necessary to foster cellular growth at the desired rate. We focused on channel $C1$ and $C3$, that is, two representative regions identified from the flow field analysis. To ensure adequate nutrient feed deep inside

Table 5. Analysis of Transport and Reaction in Perfusion Channels of Bioreactor under Study

Transport and reaction in perfusion channels			
		Channel C1	Channel C3
Channel size	d^*	1.25 mm	0.48 mm
Channel length	L	8	20.57
Perfusion flow	$4Q_i/Q_n$	8.48%	0.2%
Advective velocity	U_0	$2.26\ 10^{-4}$ m/s	$3.53\ 10^{-5}$ m/s
Nutrient concentration (O_2^*)	C_0	80% C_{sat}; $5.76\ 10^{-3}$ kg/m^3	
Nutrient target concentration (O_2^*)	C_t^{**}	0.39 Csat; $2.81\ 10^{-3}$ kg/m^3	
Dimensionless target concentration ($\tilde{O}_2^{**}$)	C_t^{**}/C_0	0.487	
Nutrient diffusivity (O_2^*)	D	$3.\ 10^{-9}$ m^2/s	
Nutrient specific flux wall (O_2^*)	R_m	$4.42\ 10^{-9}$ kg/m^{2}s	
Specific wall surface	S_w	2258 m^2/m^3	4687 m^2/m^3
Void fraction	ε	58.29%	32.18%
Peclet number (macro)	Pe_L	753.78	117.541
Damkholer number (macro)	Da_L	112.72	233.89
Peclet number (micro)	Pe	94.22	5.71
Damkholer number (micro)	Da	1.76	0.55
Min Peclet number	Pe_{min}	27.50	22.19
Min perfusion flow	$Q_{n,min}$	29.19%Q_n	388%Q_n

the side vanes ($L_{crit} = d_f/2 = 0.5$ mm) of these channels, according to Eq. 7 and using $S_w = 3200$ (see Appendix), the oxygen concentration at the entrance of side vanes should be at least $C_{0,sv} = 2.81$ mg/L. This value, indicated as O_2^{**} in Table 5, should be used as target value for the oxygen concentration at the end of each channel in the present scaffold configuration. Macroscale dimensionless transport numbers calculated for channel C1 ($Pe_L = 735.5$ and $Da_L = 112.72$) indicate transport-controlled conditions ($Da_L < Pe_L + 1$). Macroscale dimensionless transport numbers calculated for channel C3 ($Pe_L = 117.54$ and $Da_L = 233.89$) indicate reaction-controlled conditions ($Da_L > Pe_L + 1$).

Microscale Peclet and Damkholer numbers calculated based on the channel size according to the 1-D model are $Pe = 94.22$ and $Da = 1.76$ for channel C1 and $Pe = 5.71$ and $Da = 0.55$ for channel C3. Using Eq. 15, we can calculate the minimum value of Pe to be in transport-controlled conditions in each channel: we get $Pe_{min} = 27.50$ for channel C1 and 22.19 for channel C3, respectively. These values, compared with the microscale Pe evaluated at nominal perfusion flow rate, indicate that Q_n could be reduced to 29.18%Q_n still being in transport-controlled conditions in channel C1, whereas Q_n should be increased to 388%Q_n to be in transport-controlled conditions in channel C3. These results hold when $C_0 = 0.8 \cdot C_{sat}$. If the concentration in the feed changes, the perfusion flow rate should be modified accordingly. The perfusion flow necessary to meet the target concentration at the outlet of channel C1 (solid line) and at the outlet of channel C3 (dashed line) when the oxygen concentration in the feed changes is shown in Figure 10. Solid and empty symbols on the two lines identify the (optimal) working conditions when the concentration in the feed is 80%C_{sat}; the vertical line identifies the target value of concentration to be maintained at the outlet of each perfusion channel. Whichever the concentration of oxygen in the feed (x axis), the two lines identify the value of the perfusion flow rate (on the y axis) necessary to guarantee adequate nutrient supply everywhere and at the end of the channel. Values of minimal perfusion flow are larger for channel C3. Nevertheless, conditions represented by channel C3 correspond to roughly 5% of overall scaffold surface. Focusing on channel C1, the solid line can be used to identify, whichever the oxygen concentration measured in the real time by an in-line sensor at bioreactor inlet, the minimal perfusion flow required to ensure the target cellular growth rate inside the bioreactor.

Conclusions

In this work, we describe a four steps modeling approach to identify sets of culture conditions to promote homogeneous growth of cells on scaffolds surface. First, we determine the relationship between cellular growth rate and local nutrient concentration. Based on this relation, we identify threshold concentration values required to maintain the desired cell growth rate; second, we calculate macroscale dimensionless transfer numbers and we use them to identify conditions in which dynamic culturing should be used. Third, building on precise, 3-D data (flow field and shear-stress distribution), we identify regions where cellular growth may become critical due to either insufficient/excessive mechanical stimulation or inadequate nutrient supply; finally, using a 1-D mass transport and reaction model, we calculate the minimal perfusion flow necessary to maintain the cellular growth rate above a target threshold and we derive a design equation to

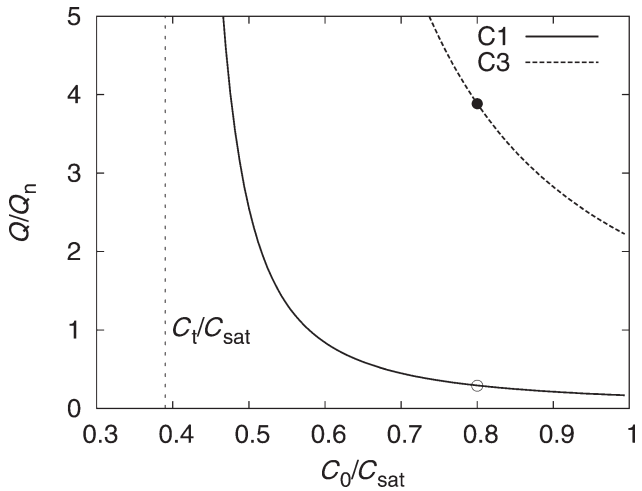

Figure 10. Minimal perfusion flow rate vs. nutrient concentration in the feed to guarantee $K = 80\%K_{max}$ all along the perfusion channels C1 (solid line) and C3 (dashed line) of bioreactor under study.

control the culturing process inside the bioreactor in the real time.

The developed approach is demonstrated by a case study in which we analyze culturing conditions inside an indirect perfusion bioreactor equipped with a lattice scaffold specifically designed to grow bone grafts. Data of cell metabolic activity collected by experiments were used together with the results of a 3-D numerical simulation of the flow field and shear stress inside the bioreactor to identify possible pitfalls in bioreactor/scaffold design and in the operating protocol. Results of the numerical simulation suggest that mechanical stimulation of cell is not a critical issue in the bioreactor under study. Results of the 1-D mass transport and reaction model suggest that the nominal perfusion flow indicated by the culturing protocol is adequate to foster cellular growth at the target rate.

Acknowledgments

Financial contribution from VivaBioCell is gratefully acknowledged. The Authors would like to acknowledge dott. Massimo Moretti and dott. Giacomo Cattaruzzi for their experimental contribution and helpful technical discussions.

Literature Cited

1. Yang L, Sun H, Qi N. A Novel mini beta-TCP 3D perfusion bioreactor for proliferation and osteogenic differentiation of bone marrow mesenchymal stem cells. *Biotech Bioprocess Eng*. 2010;15:329–340.
2. Kanczler JM, Oreffo ROC. Osteogenesis and angiogenesis: the potential for engineering bone. *Eur Cells Mater*. 2008;15:100–114.
3. Marolt D, Knezevic M, Novakovic GV. Bone tissue engineering with human stem cells. *Stem Cell Res Ther*. 2010;1:1–10.
4. Byrne DP, Lacroix D, Planell JA, Kelly DJ, Prendergast PJ. Simulation of tissue differentiation in a scaffold as a function of porosity, Young's modulus and dissolution rate: application of mechanobiological models in tissue engineering. *Biomaterials*. 2007; 28:5544–5554.
5. Provin C, Takano K, Sakai Y, Fujii T, Shirakashi R. A method for the design of 3D scaffolds for high-density cell attachment and determination of optimum perfusion culture conditions. *J Biomech*. 2008;41:1436–1449.
6. Rauh J, Milan F, Guenther KP, Maik S. Bioreactor systems for bone tissue engineering. *Tissue Eng. Part B Rev*. 2011;17:263–280.
7. Porter B, Zauel R, Stockman H, Guldberg R, Fyhrie D. 3-D computational modeling of media flow through scaffolds in a perfusion bioreactor. *J Biomech*. 2005;38:543–549.
8. Ma CYJ, Kumar R, Xu XY, Mantalaris A. A combined fluid dynamics, mass transport and cell growth model for a three-dimensional perfused bioreactor for tissue engineering of haematopoietic cells. *Biochem Eng J*. 2007;35:1–11.
9. Olivares AL, Marshal E, Planell JA, Lacroix D. Finite element study of scaffold architecture design and culture conditions for tissue engineering. *Biomaterials*. 2009;30:6142–6149.
10. McCoy RJ, Jungreuthmayer C, O'Brien FJ. Influence of flow rate and scaffold pore size on cell behavior during mechanical stimulation in a flow perfusion bioreactor. *Biotech Bioeng*. 2012;109:1583–1594.
11. Lacroix D, Planell JA, Prendergast PJ. Computer-aided design and finite-element modelling of biomaterial scaffolds for bone tissue engineering. *Phil Trans Royal Soc A*. 2009;367:1993–2009.
12. Godara P, McFarland CD, Nordon RE. Design of bioreactors for mesenchymal stem cell tissue engineering. *J Chem Tech Biotech*. 2008;83:408–420.
13. Hollister SJ. Porous scaffold design for tissue engineering, *Nature Mater*. 2005;4:518–524.
14. Kaazempur-Mofrad MR, Bathe M, Karcher H, Younis HF, Seong HC, Shim EB, Chan RC, Hinton DP, Isasi AG, Upadhyaya A, Powers MJ, Griffith LG, Kamm RD. Role of simulation in understanding biological systems. *Comput Struct*. 2003;81:715–726.
15. Voronov RS, Van Gordon SB, Sikavitsas VI, Papavassiliou DV. Computational modeling of flow-induced shear stresses within 3D salt-leached porous scaffolds imaged via micro-CT. *J Biomech*. 2010a;43:1279–1286.
16. Voronov RS, Van Gordon SB, Sikavitsas VI, Papavassiliou DV. Distribution of flow-induced stresses in highly porous media. *Appl Phys Lett*. 2010b;97. DOI: 10.1063/1.3462071.
17. VanGordon SB, Voronov RS, Blue TB, Shambaugh RL, Papavassiliou DV, Sikavitsas VI. Effects of scaffold architecture on preosteoblastic cultures under continuous fluid shear. *Ind Eng Chem Res*. 2011;50:620–629.
18. Voronov RS, Van Gordon SB, Sikavitsas VI, Papavassiliou DV. Efficient Lagrangian scalar tracking method for reactive local mass transport simulation through porous media. *Int J Num Meth Fluids*. 2011;67:501–517.
19. Flaibani M, Magrofuoco E, Elvassore N. Computational modeling of cell growth heterogeneity in a perfused 3D scaffold. *Ind Eng Chem Res*. 2010;49:859–869.
20. Hutmacher DW, Sittinger M, Risbud MV. Scaffold-based tissue engineering: rationale for computer-aided design and solid free-form fabrication systems. *Trends Biotechnol*. 2004;22:354–362.
21. Shor L, Guceri S, Wen X, Gandhi M, Sun W. Fabrication of three-dimensional polycaprolactone/hydroxyapatite tissue scaffolds and osteoblast-scaffold interactions in vitro. *Biomaterials*. 2007;28: 5291–5297.
22. Wang CC, Yang KC, Lin KH, Liu HC, Lin FH. A highly organized three-dimensional alginate scaffold for cartilage tissue engineering prepared by microfluidic technology. *Biomaterials*. 2011;32: 7118–7126.
23. Melchels FPW, Barradas AMC, van Blitterswijk CA, de Boer J, Feijen J, Grijpma DW. Effects of the architecture of tissue engineering scaffolds on cell seeding and culturing. *Acta Biomaterialia*. 2010;6: 4208–4217.
24. Boschetti F, Raimondi MT, Migliavacca F, Dubini G. Prediction of the microfluid dynamic environment imposed to three-dimensional engineered cell systems in bioreactors. *J Biomech*. 2006;39:418–425.
25. Truscello S, Kerckhofs G, Van Bael S, Pyka G, Schrooten J, Van Oosterwyck H. Prediction of permeability of regular scaffolds for skeletal tissue engineering: a combined computational and experimental study. *Acta Biomater*. 2012;8:1648–1658.
26. Van Bael S, Chai YC, Truscello S, Moesen M, Kerckhofs G, Van Oosterwyck H, Kruth JP, Schrooten J. The effect of pore geometry on the in vitro biological behavior of human periosteum-derived cells seeded on selective laser-melted Ti6Al4V bone scaffolds. *Acta Biomat*. 2012;8:2824–2834.
27. Papantoniou I, Chai YC, Luyten FP, Schrooten J. Process quality engineering for bioreactor driven manufacturing of tissue engineered constructs for bone regeneration. *Tissue Eng Part C Meth*. 2013 DOI: 10.1089/ten.tec.2012.0526.
28. Truscello S, Schrooten J, Van Oosterwyck H. A computational tool for the upscaling of regular scaffolds during in vitro perfusion culture. *Tissue Eng Part C Meth*. 2011;17:619–630.
29. Grayson WL, Marolt D, Bhumiratana S, Frohlich M, Guo XE, Vunjak-Novakovic G. Optimizing the medium perfusion rate in bone tissue engineering bioreactors. *Biotechnol Bioeng*. 2011;108:1159–1170.
30. Titmarsh D, Hidalgo A, Turner J, Wolvetang E, Cooper-White J. Optimization of flowrate for expansion of human embryonic stem cells in perfusion microbioreactors. *Biotech Bioeng*. 2011;108: 2894–2904.
31. Marolt D, Campos IM, Bhumiratana S, Koren A, Petridis P, Zhang GP, Spitalnik PF, Grayson WL, Vunjak-Novakovic G. Engineering bone tissue from human embryonic stem cells. *PNAS*. 2012;109: 8705–8709.
32. Meijer GJ, de Bruijn JD, Koole R, van Blitterswijk CA. Cell-based bone tissue engineering. *PLoS Med*. 2007;4:260–264.
33. Curcio F, Fontanini A, Cattaruzzi G, Vitrani F, Moretti M, Campolo M, Soldati A, Ambesi-Impiombato FS. Adult stem cells in therapy: a practical approach. *FASEB J*. 2012;26. WOS:000310411301391.
34. Dunn JCY, Chan WY, Cristini V, Kim JS, Lowengrub J, Singh S, Wu BM. Analysis of cell growth in three-dimensional scaffolds. *Tissue Eng Part C Meth*. 2006;12:705–716.
35. Scarbolo L, Molin D, Perlekar P, Sbragaglia M, Soldati A, Toschi F. Unified framework for a side-by-side comparison of different multicomponent algorithms: lattice Boltzmann vs. phase field model. *J Comput Phys*. 2012;234:263–279.
36. Hu Z, Lowengrub J, Wise SM, Voigtd A. Phase-field modeling of epitaxial growth: applications to step trains and island dynamics. *Phys D Nonlinear Phenomena*. 2012;241:77–94.
37. Lu SB, Sun XM, Zhang YX. Insight into metabolism of CHO cells at low glucose concentration on the basis of the determination of intracellular metabolites. *Proc Biochem*. 2005;40:1917–1921.

38. Pattappa G, Heywood HK, De Bruijn JD, Lee DA. The metabolism of human mesenchymal stem cells during proliferation and differentiation. *J Cell Physiol*. 2011;226:2562–2570.
39. Ferro F, Spelat R, Beltrami AP, Cesselli D, Curcio F. Isolation and characterization of human dental pulp derived stem cells by using media containing low human serum percentage as clinical grade substitutes for bovine serum. *PLoS One*. 2012;7:e48945. DOI: 10.1371/journal.pone.0048945.
40. Freyer JP, Sutherland RM. Regulation of growth saturation and development of necrosis in EMT6/Ro multicellular spheroids by the glucose and oxygen supply. *Cancer Res*. 1986;46:3504–3512.
41. Ferro F, Falini G, Spelat R, D'Aurizio F, Puppato E, Pandolfi M, Beltrami AP, Cesselli D, Beltrami CA, Impiombato FSA, Curcio F. Biochemical and Biophysical Analyses of Tissue-Engineered Bone Obtained from Three-Dimensional Culture of a Subset of Bone Marrow Mesenchymal Stem Cells. *Tissue Eng Part A*. 2010;16:3657–3667.

Appendix

Scaffold characterization

The geometrical structure of regular scaffolds can be characterized using two main parameters

- the specific surface area, S_w, defined as area exposed to perfusion per unit volume of fluid;
- the void fraction ε, defined as the volume open to fluid flow per unit volume of scaffold.

For a scaffold made of parallel channels (square section of size d, length L) with wall thickness d_f, the specific surface area and the void fraction are given by

$$S_w = \frac{4dL}{d^2L} = \frac{4}{d} \tag{A1}$$

$$\varepsilon = \frac{d^2L}{\left(d+d_f\right)^2L} = \frac{1}{(1+k)^2} \tag{A2}$$

where $k = d_f/d$. For a scaffold with lattice-type structure (fiber interspace d, fiber size d_f), with reference to the minimal unit volume, the specific surface area and the void fraction can be calculated as

$$S_w = \frac{12d \cdot d_f}{d^3+3d^2 \cdot d_f} = \frac{12k}{(1+3k)d} \tag{A3}$$

$$\varepsilon = \frac{(1+3k)d^3}{(1+k)^3d^3} = \frac{1+3k}{(1+k)^3} \tag{A4}$$

with $k = d_f/d$. In lattice-type scaffold, the surface per unit volume of scaffold available for cell culturing ($S_w \cdot \varepsilon$) is larger than in a scaffold with parallel channels when $k = d_f/d > 0.5$.

Channel C3 characterization

For the unit volume of scaffold corresponding to channel C3, we can calculate the following quantities

- flow area, A

$$A \simeq \frac{L_f^2}{2} \tag{A5}$$

where

$$L_f = \left(d_f/2+d\right) - d_{sc}\sin\theta/2 \tag{A6}$$

and $\theta = \pi/2 - 2\arccos\left[2\left(d_f/2+d\right)/d_{sc}\right]$

- surface area, A_w

$$A_w \simeq 4L_f d_f + d_f \cdot d + \left(d_f+d\right)d_{sc}\theta/2 \tag{A7}$$

- fluid volume, V_f

$$V_f \simeq A\left(d+d_f\right) + d_f \cdot dL_f \tag{A8}$$

- specific surface area, S_w

$$S_w = \frac{A_w}{V} \tag{A9}$$

- characteristic length, $d^* = \sqrt{A}$

Considering the values of d_{sc}, d and d_f from Table 3, we get $A = 2.3633 \cdot 10^{-7}\text{m}^2$, $d^* = 4.86 \cdot 10^{-4}\text{m}$, and $S_w = 4687.14\ \text{m}^2/\text{m}^3$.

Manuscript received Apr. 17, 2012, and revision received Feb. 4, 2013.